Journal of Biochemical and Molecular Toxicology

WILEY

RESEARCH ARTICLE OPEN ACCESS

Synthesis, Cytotoxic Activity, Antiquorum Sensing Effect, Docking and Md Simulation of Novel 1,3-Disubstituted 2-Mercapto-1*H*-Benzo[*D*]Imidazolium Chlorides

Mohammad Mavvaji[1] | Muhammed Tilahun Muhammed[2] | Ebru Onem[3] | Halime Güzin Aslan[4] | Sadeq K. Alhag[5] | Senem Akkoc[1,6]

[1]Faculty of Pharmacy, Department of Basic Pharmaceutical Sciences, Suleyman Demirel University, Isparta, Türkiye | [2]Faculty of Pharmacy, Department of Pharmaceutical Chemistry, Suleyman Demirel University, Isparta, Türkiye | [3]Faculty of Pharmacy, Department of Pharmaceutical Microbiology, Suleyman Demirel University, Isparta, Türkiye | [4]Faculty of Sciences, Department of Chemistry, Erciyes University, Kayseri, Türkiye | [5]Health Specialties, Basic Sciences and Applications Unit, Applied College, Mohayil Asir, King Khalid University, Abha, Saudi Arabia | [6]Faculty of Engineering and Natural Sciences, Bahçeşehir University, Istanbul, Türkiye

Correspondence: Senem Akkoc (senemakkoc@sdu.edu.tr; senemakkoc44@gmail.com)

Received: 21 January 2025 | **Revised:** 5 March 2025 | **Accepted:** 27 March 2025

Funding: The authors would like to thank the Erciyes University Research Fund for financial support with project number FBA-2022-11424.

Keywords: 2-mercapto-1*H*-benzo[*d*]imidazolium | Cytotoxic activity | docking studies | MD simulation | quorum sensing

ABSTRACT

A series of benzimidazolium chlorides (**2a-c**) and their corresponding 2-mercapto derivatives (**3a-c**) were proficiently synthesized and analyzed by NMR and LC-MS spectra. The in vitro cytotoxic assay demonstrated that some synthesized compounds were active on the cancer cell lines. The binding potential of the most active three compounds to topoisomerase II alpha (topo2α) was explored to unveil the possible mode of action for the cytotoxic activity. The binding potential was examined through molecular docking. The stability of compound-enzyme complexes from docking was investigated through molecular dynamics (MD) simulation. The docking study revealed that the three compounds (**3a-c**) showed the ability to bind to the enzyme. However, the binding strength of compounds was weaker than that of the standard drug, doxorubicin. The MD simulation analysis demonstrated that compounds **3a** and **3b** gave relatively stable complexes with the enzyme and thus they would remain inside the binding pocket during the simulation period. Furthermore, the pharmacokinetic properties of the relatively active compounds were computed *in silico*. The computation disclosed that all of compounds exhibited drug-like properties. It is worth mentioning that all of them were found to be nontoxic. In furtherance, the inhibitory effect of compounds (**3a-c**) on the quorum sensing system was inspected using the biomonitor strains *Chromobacterium violaceum* 026, *Chromobacterium. violaceum* VIR07 and *Pseudomonas aeruginosa* PAO1. In this regard, we focused on the appraisal of the virulence factors, including pyocyanin, elastase, and biofilm formation that are created by *P. aeruginosa* PAO1 as the source of infectious diseases. As a result, it was determined that all examined compounds displayed statistically significant inhibition effects, and the highest activity was observed on elastase production with an inhibition rate of 84–86%.

1 | Introduction

Since the past couple of decades, benzimidazole derivatives have garnered significant attention due to their diverse biological and therapeutic properties [1–5]. As a critical component in pharmaceutical development, benzimidazoles exhibit a wide range of pharmacological activities and play a key role in the formulation of various drugs [6]. The benzimidazole

framework is particularly notable for meeting essential structural requirements in pharmacological applications [7–9]. The benzimidazole scaffold exhibits a significant structural similarity to natural nucleotides, enabling effective interactions with the active sites of biopolymers in biological systems. Notably, the resemblance between 2-aminobenzimidazole and purine highlights the potential of these frameworks for diverse biological applications [10]. In this trend, the substantial anticancer competences of benzimidazole-based structures have enticed a great deal of interest in recent years, giving rise to the growth of appreciable benzimidazole-bearing medications that have strikingly influenced the progress of modern cancer-combatting approaches [11–15]. Besides, the profitability of benzimidazole derivatives to suppress the function of manifold enzymes broadened the boundaries for remedying copious deadly diseases, with distinct emphasis on myriad sorts of cancer [16]. Apropos to the subject, benzimidazole-containing skeletons can competently impede the thriving of cancer cells with the aid of multifactorial strategies entailing the inhibition of enzyme behavior, alteration of mitochondrial operation, antiproliferative and apoptosis processes, by the joint action of obstructing cell cycle sequence (predominantly by interrupting the G1 and G2/M phase) [17–20]. Among the varied benzimidazole-bearing species, 2-mercaptobenzimidazoles are taken into account as worthwhile intermediates for the manufacture of innovative biologically active frameworks. These scaffolds endow a broad range of therapeutic potencies *e.g.* antitumor, anti-Alzheimer, anti-inflammatory, antibacterial, and anticancer features [21, 22]. Meanwhile, di-substituted benzimidazole derivatives are contemplated as a pivotal group of benzimidazoles due to their widespread proficiencies in the scope of biology and pharmaceuticals [23–25]. On this account, the elaborate design and creation of these valuable compounds, coupled with the estimation of their curative capabilities are of extreme significance.

Incorrect and unnecessary usage of antibiotics in the treatment of bacterial infections has made it difficult to combat these diseases and has led to an increase in mortality, especially in nosocomial infections [26]. Understanding that the system known as quorum sensing (QS) plays a crucial role in the activation of virulence factors in pathogenic microorganisms has sparked a growth in efforts to disrupt this system in the fight against such microorganisms [27]. In other words, antibacterial drug discovery research in the past 20 years have been centered on blocking QS, a signaling process that bacteria utilize to control the expression of virulence traits and resistance to antibiotics [28]. In Gram-negative bacteria, such signaling molecules are usually *N*-acylhomoserine lactones (AHLs). These signaling molecules are employed to examine the virulence properties of bacteria [29]. Therefore, numerous microorganisms exploit this system and as noticeable instances, it is operative in the virulence of *C. violaceum* and *P. aeruginosa*. In the case of *C. violaceum*, this process is screened via forming violet colored colonies in the medium. This violet color originates from the *violacein* pigment, a secondary metabolite produced by the bacterium [30]. Additionally, *violacein* purple pigment is applied in studies as a measurable agent for quorum sensing activity [31]. *P. aeruginosa* is another Gram-negative pathogenic bacterium that causes serious infections in humans, peculiarly in immunosuppressed patients. It contains several virulence factors such as *pyocyanin*, a blue-green metabolite. *P. aeruginosa* actively exerts a virulence mechanism similar to *C. violaceum*, chiefly through the generation of *pyocyanin* pigment, elastase enzyme production, as well as biofilm formation [32].

In very recent work, we explored the cytotoxic capability, and molecular docking survey of novel benzimidazolium chlorides [33]. Encouraging by these promising results and in continuation of our earlier works on synthesizing and appraising the cytotoxic effects of benzimidazole-based compounds [34–41], in the present study, we explored the synthesis of new *N*,*N*-disubstituted benzimidazolium chlorides (**2b** and **2c**) and their corresponding novel 2-mercapto-benzimidazolium salts (**3a-c**), alongside the analysis of their inhibitory and cytotoxic effects. To enhance our comprehension of the binding affinities of the prepared compounds, we applied molecular docking and molecular dynamics simulation techniques.

2 | Experimental

2.1 | Synthesis and Characterization of New Compounds

2.1.1 | Synthesis of 1,3-disubstituted Benzimidazolium Chlorides

The synthesis of the 1,3-disubstituted benzimidazolium salts (**2a-c**) was performed (Scheme 1) [33, 42]. A mixture of 2-chlorobenzimidazole (152.58 mg, 1 mmol) and DMF (5 mL) was cooled to 0°C, followed by the addition of sodium hydride (NaH, 28.8 mg, 1.2 mmol). Benzyl chloride (2.2 mmol) was then introduced, and the reaction mixture was stirred at room temperature for 36 h. The compounds were verified by NMR spectroscopy.

2.1.2 | Synthesis of 1,3-disubstituted-2-mercapto-benzimidazolium Chlorides

The desired disubstituted-2-mercapto-benzimidazolium salts (**3a-c**) were successfully achieved through the following procedure (Scheme 1) [42]. A solution of benzimidazolium chloride (**2a-c**, 0.21 mmol) in DMF (3 mL) was prepared and upon addition of sodium sulfide (Na_2S, 0.74 mmol), the mixture was kept to stir up under heating (100°C) for 5 h. Then, the chilled water was added to the reaction mixture and the acquired precipitate was filtered and rinsed several times with deionized water (10 mL). In the last step, the pure product was obtained as a white solid after recrystallization from DMF:H_2O. These new thiol compounds (**3a-c**) were identified via ^{1}H NMR, ^{13}C NMR, and LC-MS spectra.

2.1.3 | Characterization Data of Synthesized Compounds

2.1.3.1 | 1,3-Dibenzyl-2-Chloro-1*H*-Benzo[*D*]imidazol-3-ium Chloride (2A). Yield, melting point, ^{1}H NMR, and ^{13}C NMR information are given in the literature [33].

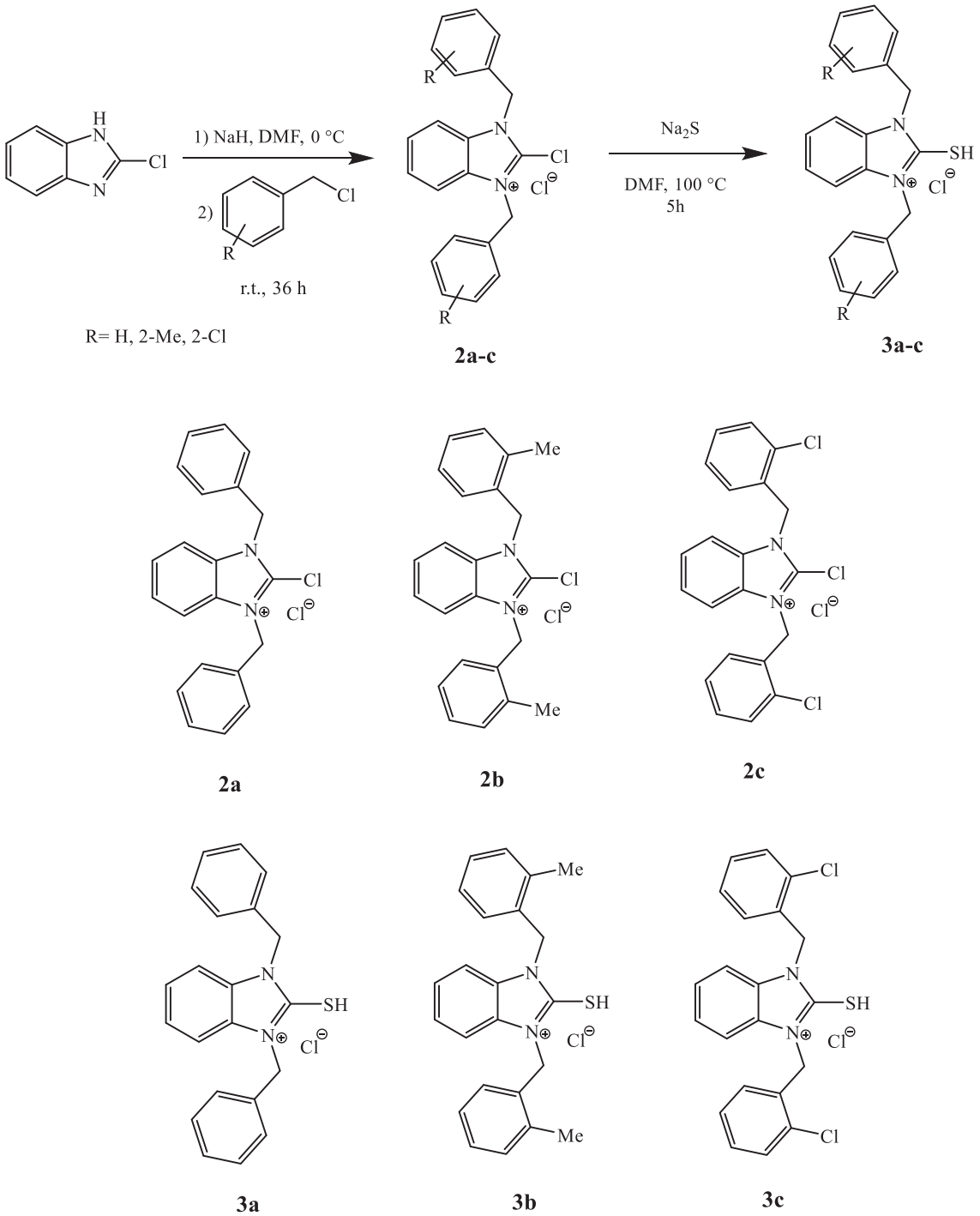

SCHEME 1 | Synthetic path for the manufacture of di-substituted-2-mercapto-benzimidazolium chlorides (**3a-c**).

2.1.3.2 | 2-Chloro-1,3-Bis(2-Methylbenzyl)-1*H*-Benzo[*D*] imidazol-3-ium Chloride (2B). Pale yellow solid; Yield: 64%; M.p.: 189–191°C. ^{1}H NMR (400 MHz, $CDCl_3$, δ, ppm): 7.76 (d, $J = 8.0$ Hz, 1H), 7.21–7.32 (m, 4H), 7.05–7.13 (m, 2H), 6.66 (d, $J = 7.2$ Hz, 1H), 5.45 (d, $J = 7.0$ Hz, 2H), 2.43 (s, 3H). ^{13}C NMR (100 MHz, $CDCl_3$, δ, ppm): 141.81, 141.14, 135.30, 135.02, 132. 81, 130.67, 127.97, 126.57, 125.77, 123.38, 122.90, 119.56, 109.97, 46.04, and 19.21.

2.1.3.3 | 2-Chloro-1,3-Bis(2-Chlorobenzyl)-1*H* Benzo[*D*] imidazol-3-ium Chloride (2C). Yellow solid; Yield: 59%; M.p.: 197–199°C. ^{1}H NMR (400 MHz, $CDCl_3$, δ, ppm): 7.78 (t, $J = 8.0$ Hz, 1H), 7.47 (d, $J = 8.0$ Hz, 1H), 7.13–7.33 (m, 5H), 6.63 (d, $J = 8.0$ Hz, 1H), 5.52 (s, 2H). ^{13}C NMR (100 MHz, $CDCl_3$, δ, ppm): 141.30, 140.93, 134.93, 132.39, 132.35, 129.85, 129.62, 129.37, 128.85, 128.19, 127.45, 127.20, 123.75, 123.29, 121.86, 121.68, 119.50, 109.88, 109.34, 45.48, and 41.90.

2.1.3.4 | 1,3-Dibenzyl-2-Mercapto-1*H*-Benzo[*D*] imidazol-3-ium Chloride (3A). White solid; Yield: 71%; M.p.: 190–192°C. ^{1}H NMR (400 MHz, $CDCl_3$, δ, ppm): 10.03 (s, 1H), 8.15 (d, $J = 8.0$ Hz, 1H), 7.69 (d, $J = 8.0$ Hz, 1H), 7.34–7.56 (m, 11H), 7.11–7.23 (m, 1H), 5.74 (s, 2H), 5.56 (s, 2H). ^{13}C NMR (100 MHz, $CDCl_3$, δ, ppm): 128.94, 128.86, 127.99, 127.64,

127.57, 126.96, 126.91, 123.75, 123.28, 110.06, 29.43, and 26.35. LC-MS = m/z: $[M-Cl]^+$ Calcd for $C_{21}H_{19}N_2S$, 331.41; Found: 331.10.

2.1.3.5 | 2-Mercapto-1,3-Bis(2-Methylbenzyl)-1*H*-Benzo[*D*]imidazol-3-ium Chloride (3B). White solid; Yield: 63%; M.p.: 194–196°C. ^{1}H NMR (400 MHz, $CDCl_3$, δ, ppm): 10.07 (s, 1H), 7.29–7.38 (m, 7H), 7.11–7.22 (m, 3H), 6.83-6.89 (m, 2H), 5.57 (s, 2H), 5.45 (s, 2H), 2.44 (s, 6H). ^{13}C NMR (100 MHz, $CDCl_3$, δ, ppm): 135.52, 132.94, 132.83, 130.63, 127.65, 126.34, 123.51, 123.06, 110.07, 109.82, 46.11, and 19.40. LC-MS = m/z: $[M-H]^+$ Calcd for $C_{23}H_{23}ClN_2S$, 393.96; Found: 393.30.

2.1.3.6 | 2-Mercapto-1,3-Bis(2-Chlorobenzyl)-1*H*-Benzo[*D*]imidazol-3-ium Chloride (3C). White solid; Yield: 56%; M.p.: 204–207°C. ^{1}H NMR (400 MHz, $CDCl_3$, δ, ppm): 10.29 (broad s, 1H), 7.46 (t, $J = 8.0$ Hz, 2H), 7.29–7.32 (m, 3H), 7.20–7.25 (m, 4H), 7.03–7.13 (m, 2H), 6.63 (d, $J = 8.0$ Hz, 1H), 5.69 (s, 2H), 5.52 (s, 2H). ^{13}C NMR (100 MHz, $CDCl_3$, δ, ppm): 132.64, 129.65, 129.29, 128.99, 128.08, 127.42, 127.29, 123.74, 123.27, 109.88, 109.78, and 44.89. LC-MS = m/z: $[M-Cl-H]^+$ Calcd for $C_{21}H_{16}Cl_2N_2S$, 399.30; Found: 399.05.

2.2 | Molecular Docking

The structure of human topoisomerase II alpha (topo2α) was retrieved from the protein data bank (PDB). The crystal structure of topo2α (PDB code: 5GWK) had etoposide embedded inside it [43]. The molecular docking was undertaken by AutoDock Vina. The compounds were drawn by ChemDraw Professional and the standard drugs were obtained from PubChem [44]. The docking was performed as described in previous studies [45, 46]. The resulting computation was visualized by Biovia Discovery Studio and then analyzed accordingly.

2.3 | Molecular Dynamics Simulation

Molecular dynamics (MD) simulation of the relatively active derivatives and the standard drug, doxorubicin, were performed to unveil the stability of enzyme-compound complexes retrieved from the docking. MD simulations were done by using the GROMACS (Groningen Machine for Chemical Simulations) package as reported in earlier studies [47, 48]. Then, root mean square deviation (RMSD) plots for the enzyme and the compounds, root mean square fluctuation (RMSF), and Rg (radius of gyration) plots were drawn through qtgrace and analyzed accordingly.

2.4 | *In silico* Pharmacokinetic Computation

The ADMET (absorption, distribution, metabolism, elimination, toxicity) properties of the relatively active compounds were computed as *in silico*. The computation was performed by using the Accelrys Discovery Studio 3.5 program and SwissADME server [49]. AlogP98 (atomic logarithmic partition coefficient), PSA-2D (polar surface area-2 dimensional), BBB (blood-brain barrier) permeability level, bioavailability score, obeying by Lipinski's rule of five, and Ames mutagenicity values were computed. The results obtained from the two methods, Discovery Studio and SwissADME, were compared to each other. In this way, it was aimed to confirm the results by using two different methods. Some of the parameters were computed by either method.

2.5 | MIC (Minimum Inhibitor Concentration) Determination by Microdilution Method

Since Quorum sensing activity tests will be performed at concentrations that do not have a lethal effect on bacteria, the microdilution method was used to determine the MIC values of the synthesized compound [50]. In this method, 96-well microplates were prepared. For this, 100 μL of the substance and Mueller Hinton broth medium were placed in the wells, twofold serial dilutions were made, respectively, and 5 μL of the bacterial suspension prepared according to 0.5 McFarland (10^8/mL) turbidity was added. The microplates were incubated at 37/30°C overnight and the microplates were evaluated following the incubation. The smallest concentration at which no growth occurred was determined as the minimum inhibitory concentration (MIC) value and was used in the studies.

2.6 | Testing the Quorum Sensing System Inhibitory Properties of Synthesized Molecules

2.6.1 | C. violaceum 026 and C. violaceum VIR07 Pigment Production Test

The antiquorum sensing activity of the synthesized molecules was performed by pigment inhibition test on mutant forms of *C. violaceum* [51]. In this context, firstly, *C. violaceum* 026 and *C. violaceum* VIR07 strains were grown in liquid medium at 30°C for 14–16 h. First, add OdDHL N-(3-oxododecanoyl)-L-homoserine lactone for *C. violaceum* VIR07 into 5 mL soft agar; for *C. violaceum* 026, 5 μL of OHHL N-(3-oxohexanol)-L-homoserine lactone was added. Finally, 100 μL of bacterial cultures were added and transferred onto the solid medium. Then, the wells were opened with sterile 6 mm diameter glass pasteur pipettes, and 50 μL of the molecules to be studied were loaded into the wells. The next day, a possible colorless zone around the wells was evaluated as inhibition of the system.

2.7 | *P. aeruginosa* PAO1 Virulence Factors Production Tests

2.7.1 | Elastase Test

Elastase inhibition activities of the synthesized molecules were examined by the Elastin Congo Red (ECR) test [52]. Firstly, *P. aeruginosa* PAO1 was added to 10 mL LB liquid medium so that the final concentration of the synthesized compounds in the medium was 0.4 mg. It was then incubated at 37°C in a shaking incubator for 14–16 h. After incubation, 900 μL of ECR buffer (100 mM Tris, 1 mM $CaCl_2$, pH 7.5, 20 mg ECR) was added to 100 μL of the supernatant of these cultures and

incubated at 37°C for 3 h at 200 rpm. ECR that did not dissolve after incubation was removed by centrifugation and the supernatant was read at OD 495 nm. The results were compared with the positive control PAO1.

2.7.2 | Pyocyanin Test

For the inhibitory effect of compounds on pyocyanin pigment production, PAO1 was produced in LB medium at 37°C for 16–18 h [53]. The compounds to be tested were added to the bottles with 10 mL LB medium, with a final concentration of 0.4 mg. *P. aeruginosa* PAO1 strain was produced by adjusting the OD at 600 nm to be 0.02, then adding it to the bottles where the molecules were added and shaking it for 16–18 h at 37°C. At the end of the incubation, 5 mL of chloroform was added to the overnight cultures and vortexed for 30 s. The same amount of each sample was taken and placed in glass tubes, with the phase separate from chloroform at the bottom of the bottles being 2 mL. Then, 1 mL of HCL-water mixture was added to the glass tubes and vortexed for 30 s, and the pink phase formed at the top of the tubes was recorded by reading the OD at 520 nm.

2.7.3 | Biofilm Formation Test

The inhibitory activity of the synthesized compounds on biofilm formation was determined by the crystal violet test [54]. For this purpose, the overnight PAO1 culture and the concentration of the synthesized molecules to be studied were added to the microplate wells containing 200 μL LB broth medium. After 48 h of incubation, the contents of the plates were discarded and washed 3–5 times with distilled water. Then, 200 μL of 0.1% crystal violet solution was added to the wells. The contents of the wells, which were treated with crystal violet for 30 min, were emptied and washed again with pure water 3–5 times. After the washing process was completed, 200 μL 95% ethanol added each well and after 15 min the results were read at 570 nm using the "Epoch Microplate Spectrophotometer".

2.8 | Cytotoxic Activity Studies

Cell culture experiments were conducted following established protocols in the literature [34, 36–38, 40, 41]. Colon (DLD-1; ATCC® CCL-221™), lung (A549; ATCC® CCL-185™) and liver (HepG2; ATCC® HB-8065™) cancer cells were cultured in DMEM supplemented with 10% fetal bovine serum and 1% glutamax. Cells were seeded in 96-well plates at 5×10^3 cells per well. The compounds were applied to the cells at concentrations of 300, 150, 75, 37.5 and 18.75 μM and the cells were incubated for 48 h. After the 48-h period had expired, the medium was carefully transferred away. 50 μL of MTT stock (5 mg/mL) was added to the wells and waited for another 2 h. After the 2-h incubation period was reached, the medium in the wells was gently aspirated one by one with a pipette, and 200 μL dimethylsulfoxide was added to the wells to dissolve the formazone. It was left to mix in a dark environment for half an hour. Then, absorbance values were measured with an Epoch 2 Elisa plate reader at 590 nm wavelength. IC_{50} values were calculated using GraphPad Prism Software 5.

3 | Result and Discussion

3.1 | Synthesis of Compounds

The prepared benzimidazolium chlorides (**2a-c**) and corresponding 2-mercapto products (**3a-c**) were precisely analyzed by ^{1}H and ^{13}C NMR assignments using $CDCl_3$ as solvent. The illustrative synthetic scheme of the synthesized compounds is depicted below (Scheme 1). In the ^{13}C NMR spectra of 2-mercapto benzimidazolium salts, the characteristic peak of the imino carbon emerged at 128.86, 132.83 and 129.65 ppm, respectively. ^{1}H NMR spectra of the obtained 2-mercapto products displayed singlet peak, pertained to the proton of S-H bond, at 10.03, 10.07 and 10.29 (as a broad singlet) ppm. The aromatic hydrogens of the compound **3a** were observed in the range of 8.15–7.11 ppm. In the cases of **3b** and **3c**, the protons of phenyl rings were recognized within the area of 7.38–6.83 and 7.46–6.63, respectively. Additionally, the benzylic hydrogens of **3a-c** were detected as two singlet peaks in the extent of 5.74–5.56 (for **3a**), 5.57–5.45 (for **3b**) and 5.69–5.52 (for **3c**) ppm. Moreover, the singlet peak attributed to the protons of methyl groups in the compound **3b** is simply perceivable at 2.44 ppm.

3.2 | Molecular Docking

The experimental study demonstrated that some of the synthesized compounds had cytotoxic effect on the cancer cell lines. DNA topoisomerases are widely used therapeutic targets in elucidating anticancer effect mechanism of cytotoxic agents. Topoisomerase II play a substantial role in arranging DNA tangles and supercoils by cutting the two strands of the DNA helix during its metabolic processes [55]. Two isoforms of human topoisomerase II, namely topo IIα and β, are available. The two isoforms accomplish similar functions. Together with this, the two isoforms might also accomplish different functions. In this respect, topo IIα is essential for cell proliferation, but topo IIβ is not except aspects of nerve growth [56]. Hence, topo IIα is a more attractive target in designing novel anticancer agents. As a result, binding potentials of the relatively active compounds to selected topo IIα structure have been performed to elucidate their probable mode of action.

The binding potential of the relatively active compounds to topo2α was explored via molecular docking. Before proceeding to docking study of the compounds, binding potential of etoposide to the enzyme was assessed. Etoposide interacted with the enzyme via four conventional hydrogen bonds (Ade12(2), Gua13, Met766) and seven other interactions (Cyt8, Thy9, Ade12(2), Gua13(2), Arg487). A previous crystallographic study revealed that the cleavage complex that lead to DNA cleavage and thus cancer cell death was formed by the interplay of etoposide with the protein and DNA [57]. Therefore, the standard drug was bound to both the DNA and protein to be a potent inhibitor of the topo2α. The interaction of the drug with Met766

residue of the protein was found to be critical in a previous structural modeling study [43]. In this computational study, etoposide had interactions with the different subunits of the DNA as well the protein structure. This was in line with the previous study to form the cleavage complex. The essential interaction with the Met766 residue of the protein, which was reported previously, was also attained in this study that supported the findings of the study. In addition to this, among the investigated compounds, the least binding energy value was recorded for etoposide (Table 1). This result demonstrated the high binding affinity of etoposide to the human topo2α. In short, the computational study findings were in line with the previous crystallographic structural analysis. The compatibility of the docking results of etoposide lead us to pursue the computation of the active compounds and the standard drug with this protocol.

After the docking process was validated by re-docking of the etoposide complexed in the crystal structure utilized, the binding potential of the relatively active compounds as well as the standard drug, doxorubicin, was explored. The binding potential of the compounds was compared to the binding potential of the doxorubicin. Doxorubicin had the strongest interaction among the analyzed ligands as it formed seven conventional hydrogen bonds and four other types of interactions with the topo2α (Table 1, Figure 1). Doxorubicin is a well-known topoisomerase inhibitor [58]. Therefore, the high interaction of the drug with the human topo2α is in line with the literature. The high hydrogen bonding might be correlated to the high number of oxygen atoms in its structure. However, etoposide has also similar number of hydrogen atoms in its structure but the number of hydrogen bonds for doxorubicin was still higher (three more conventional hydrogen bonds) (Table 1, Figure 1).

The relatively active three compounds interacted with the human topo2α but weaker than the standard drug. They formed just a conventional hydrogen bond and at least six other types of interactions. The hydrogen bond was formed between the thiol group in their structure and different nucleotides in the crystal structure (Figure 1). All of them had interactions with the various grooves of the DNA and the protein. In this regard, their interactions were compatible with the previous crystallographic study that pointed out the importance of such binding in cleavage complex formation [57]. In another study, the importance of the interaction with the Met766 residue was pointed out [43]. Compounds **3b** and **3c** met this requirement. The binding strength and binding residues for the three compounds was similar with each other. The interaction residues of the compounds were different from that of doxorubicin. Together with this, their interaction residues had similarity with the interaction of the etoposide. Accordingly, the interactions at residues Cyt8, Thy9, Gua13, and Arg487 were common to the three investigated compounds and etoposide (Table 1, Figure 1). The binding energies of the compounds were similar with each other, compound **3a** having slightly higher value. Their binding energy values were similar to that of doxorubicin (Table 1). Therefore, their binding affinity is expected to be similar to it. Together with this, their binding strength was found be weaker than the standard drug. The compounds were found to be moderately active on the cancer cell lines in the in vitro study. As result, the interaction, which was weaker than the standard drug, confirmed their moderate anticancer activity. The findings in the docking study were also supported by a further MD simulation study.

The docking study results emphasized the role of the mercapto group in the interaction of the relatively active compounds to the topo2α target. Because a conventional hydrogen bond was formed between the compounds and the target structure with the participation of the mercapto group (Figure 1). The benzo [*d*]imidazole heterocyclic ring also involved in a number of non-hydrogen bond interactions. In this regard, compounds **3a** and **3c** formed five interactions with the involvement of this heterocyclic ring. The substituted phenyl rings also took part in the interaction of the compounds to the target structure but their level of interaction was lower than that of the heterocyclic ring generally. With this being noted, the phenyl rings of compound **2b** had comparable interaction numbers to the heterocyclic ring (Figure 1).

TABLE 1 | Binding residues of the compounds and standard drugs to the human topo2α.

Compounds	Binding Affinity (kcal/mol)	Conventional Hydrogen Bonding Residues	Other Interaction Residues
3a	−8.6	Thy9	Cyt8(2)[a], Thy9(2)[a], Gua13(2)[a], Ade12[b], Arg487[a]
3b	−9.1	Gua13	Gua7[a], Cyt8[a], Cyt8[c], Thy9[a], Arg487[a], Met766[d]
3c	−9.1	Thy9	Cyt8(2)[a], Thy9(2)[a], Ade12[b], Gua13(2)[a], Arg487[a], Met766[b]
Doxorubicin	−9.0	Gua2, Cyt3(2), Cyt4, Gua17, Ser497, Gln500	Cyt3[d], Cyt4[d], Lys499[a], Gln500[a]
Etoposide	−11.0	Ade12(2), Gua13, Met766	Cyt8[a], Thy9[e], Ade12(2)[a], Gua13(2)[a], Arg487[d]

[a]Pi-pi.
[b]pi-Sulfur.
[c]pi-ion.
[d]pi-alkyl.
[e]carbon hydrogen bond.

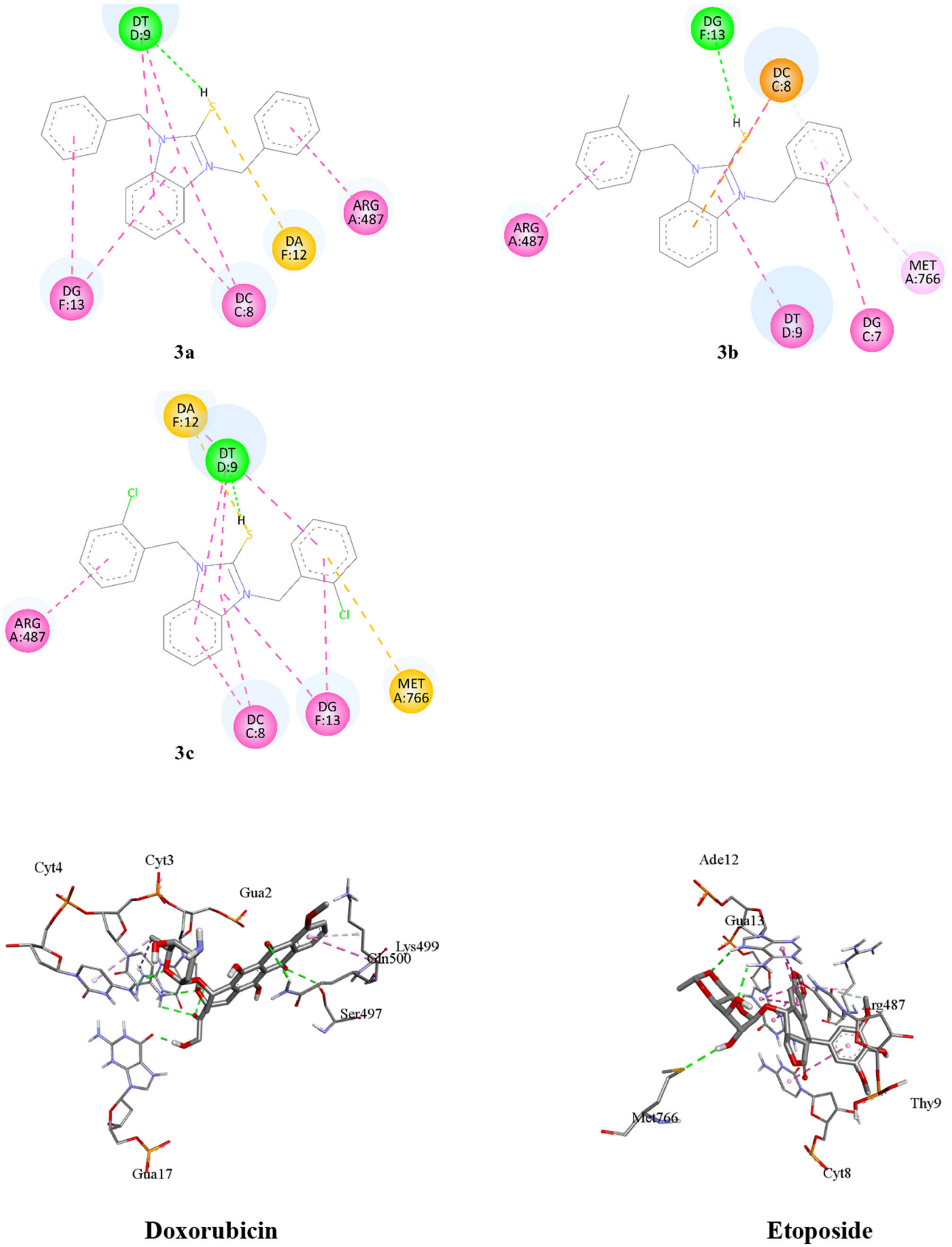

FIGURE 1 | Binding profile of the most active compounds and standard drugs with the human topo2α.

3.3 | MD Simulation

MD simulation of the relatively active compounds was undertaken and the stability of the resulting complexes was compared to the stability of the standard drug. First, RMSD value of the enzyme in relative to reference frame was utilized to measure their stability [59]. The changes in the RMSD value of all the complexes remained in a range of 0.2-0.7 nm. The enzyme structure that comprised **3c** exhibited a comparatively higher RMSD changes as well as values during the simulation period. On the other hand, the complex consisting **3b** disclosed the lowest RMSD value during the simulation period. The doxorubicin and **3a** containing complexes gave RMSD values in between (Figure 2). As the values obtained were in an acceptable range, the backbone enzyme structures were anticipated to be stable during the simulation period. Together with this, the **3b** containing backbone structure is expected to have relatively higher stability.

The RMSD plots of the compounds in the complexes were drawn to unveil their status during the simulation period. The standard drug was found to be unstable inside the binding pocket. It had relatively high RMSD value and its value changed much (Figure 2). The plot displayed also sharp rises and falls. From the RMSD plot of the standard drug, it is possible to infer that the compound has been flying out of the binding pocket. The **3c** bearing complex demonstrated greater RMSD value than the other two compounds' complex. Especially, around the twelfth ns the graph occurred a stiff rise that implied instability for it. Thereafter, the compound had relatively similar RMSD value but still much higher than the value of **3a** and **3b** bearing complexes. In general, the enzyme complexes with **3a** and **3b** embedded inside manifested similar RMSD plots during the simulation. With this being said, **3a** containing complex showed slightly lower RMSD value and thus enhanced stability during the simulation period (Figure 2). The MD simulation study clarified that compounds **3a** and **3b** would remain inside the binding pocket during the simulation period.

The per residue fluctuations during the simulation period were measured by RMSF values. The four complexes revealed similar RMSF trends. Significant fluctuations for the enzyme was recorded in 463–483, 575–630, 665–695, 918–974, 1050–1084, and 1128–1146 amino acid intervals as well as the terminals. The **3b** containing complex had significant fluctuations in the 825–835 interval. Similarly, the **3a** containing complex had unique significant rise in the 1089–1123 interval (Figure 2). The influence of the binding of compounds on the structural compactness of the enzyme was measured through Rg value [60]. The general trend for the Rg plots of the complexes was similar with nearly 3.4 nm average. Additionally, the **3c** bearing complex unveiled the highest Rg value whereas the **3b** bearing complex displayed the lowest Rg value during the simulation period (Figure 2). From these results, it is possible to infer that the enzyme-**3b** complex would have the highest compactness among these complexes. To wrap up, the MD simulation study revealed that compounds **3a** and **3b** gave relatively stable complexes and the compounds would remain inside the binding pocket during the simulation period.

3.4 | *In silico* Pharmacokinetic Properties

The relatively active compounds had suitable pharmacokinetic properties to be used as drug candidates. The compounds are anticipated to exhibit good oral absorption or permeability for oral administration. All of the compounds violated just one of the criteria of Lipinski's rule of 5 (RO5). They violated the rule that states the logP value should not exceed 5. Compound **3a** had the lowest AlogP98 value in the Discovery Studio computation (Table 2). The compounds were found to have drug-like properties for oral administration as they violated just one rule and one rule violation is allowed for compounds to be compliant to the RO5 [61].

PSA-2D values of all the compounds were found to be much lower than hundred (Figure 3). This has implicated that the compounds have good oral absorption or membrane permeability. The AlogP98 values of the compounds were above five. Compound **3a** overpassed the limit slightly (Figure 3). This result showed that the lipophilic property of most of the compounds would be not an ideal one for a drug candidate. On the other hand, the BBB barrier is expected to be permeable to all of the active compounds (Table 2). The toxicity of the compounds was tested via the Ames mutagenicity. The *in silico* computation revealed that all of the tested compounds would be non-mutagenic (Table 2).

3.5 | *C. violaceum* 026 and *C. violaceum* VIR07 Pigment Production

Imidazole compounds have been shown in several studies to have antibacterial and other therapeutic benefits, however there is a glaring lack of research on their use as anti-quorum sensing agents [62].

The mutant form of *C. violaceum* is 026, cannot produce C6-HSL but becomes capable of producing violacein with C6-HSL added to the medium. Purple pigment production in *C. violaceum* 026 strain is induced by the *N*-acyl chain between C4 and C8. The VIR07 strain, which is also a mutant of *C. violaceum* 12472, becomes capable of producing violacein pigment when long-chain AHL (C10 - C16) is added to the medium [63]. As a result of the test conducted with mutant *C. violaceum* 026 and *C. violaceum* VIR07 strains, which can produce pigment in the presence of the signal molecule, purple violaceum pigment production was observed in the petri dishes prepared by adding the signal molecule to the medium, and by opening a well on the medium, the inhibition effect of the compounds investigated on the production of violacein pigment resulted in a colorless zone around the well (Figure 4).

3.6 | Effect of Compounds on Elastase Production

According to the elastase test results, a strong inhibition effect of 86%, 84% and 85% was observed in all 3 synthesized molecules (**3a**, **3b**, **3c**). In *P. aeruginosa* some virulence factors like pyocyanin, elastase is regulated by the Rhl, Las systems, respectively [64]. Our findings suggested that **3a**, **3b**, and **3c** suppress the expression of elastase possibly by inhibiting the lasB gene (Figure 5).

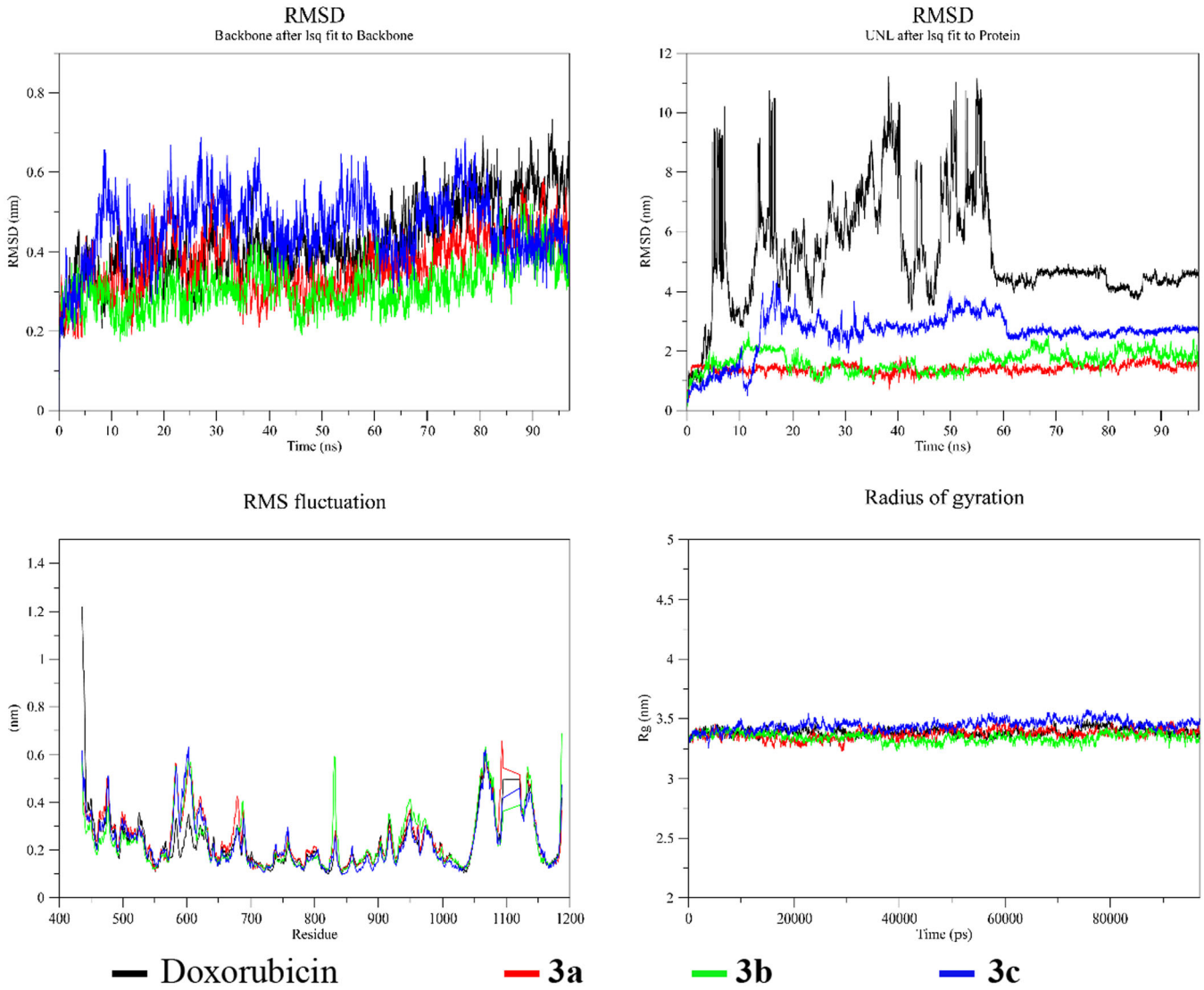

FIGURE 2 | RMSD plots of the backbone enzyme as well as the compounds, RMSF, and Rg plots from the MD simulation.

TABLE 2 | ADMET properties of the compounds.

Compound	AlogP98	PSA-2D	BBB level	Bioavailability Score	Lipinski Rule violations	Ames mutagenicity
3a	5.722	10.696	0	0.55	1	Non-mutagen
3b	6.694	10.696	0	0.55	1	Non-mutagen
3c	7.051	10.696	0	0.55	1	Non-mutagen

3.7 | Effect of Compounds on Pyocyanin Pigment Production

Pyocyanin pigment production, which is characteristic of *P. aeruginosa*, is another virulence factor that works with QS system control. In patients with cystic fibrosis, pyocyanin, an extracellular redox active virulence component of *P. aeruginosa*, promotes inflammation [65, 66]. It was observed that all of the compound whose effects were investigated had statistically significant inhibition effects in the range of 56, 57, 56% on pyocyanin production at the studied concentration (Figure 6).

3.8 | Effect of Compounds on Biofilm Formation

The inhibitory effect of the compounds **3a-c** on the biofilm formation of *P. aeruginosa* PAO1 was investigated at a concentration of 0.4 mg, and inhibition rates were obtained ranging from 44% to 56%. The detected inhibition percentages were found to be statistically significant ($p \leq 0{,}01$) (Figure 7). In a study in which a series of benzoheterocyclic sulfoxide derivatives were synthesized, the biofilm inhibition effect on PAO1 was examined and it was found that molecules containing benzoheterocyclic oxazole showed more inhibitory impacts

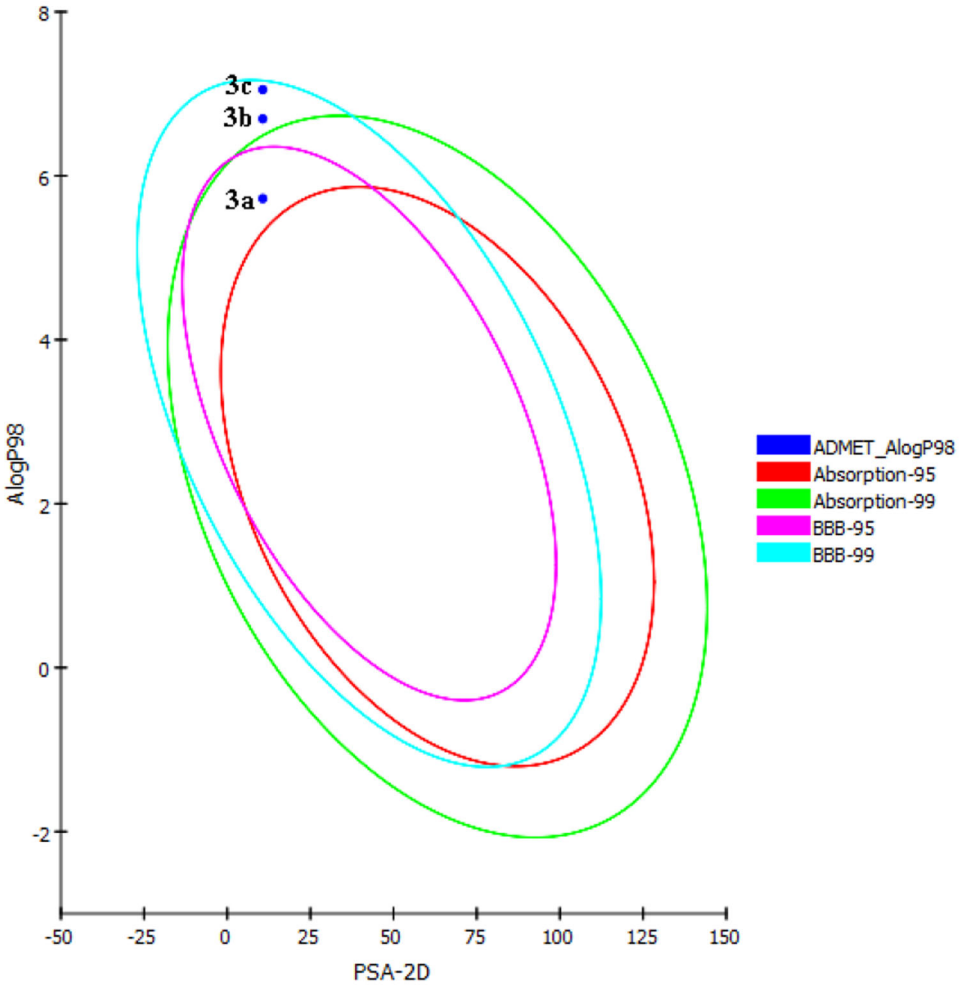

FIGURE 3 | AlogP98-PSA-2D graph of the active compounds (**3a**, **3b**, **3c**).

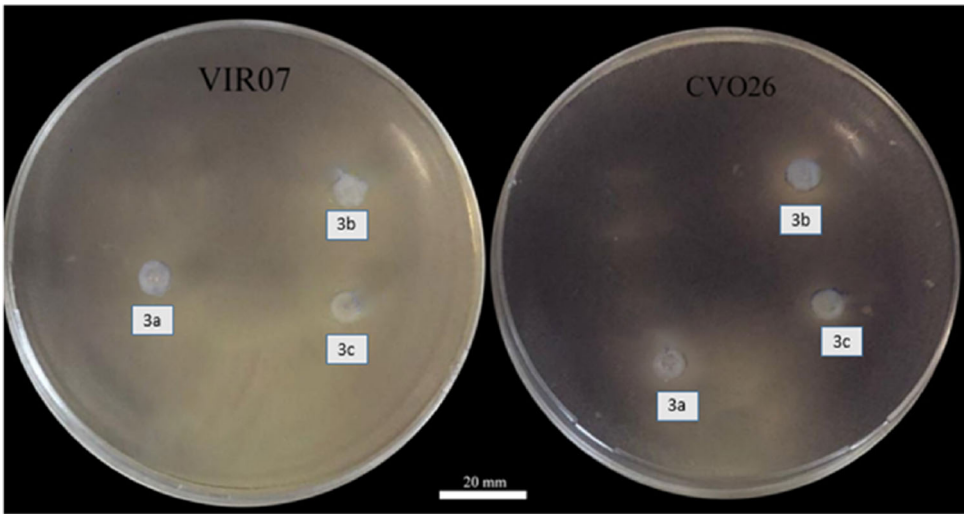

FIGURE 4 | QSI activity of compounds on CV 026, VIR07.

than benzoheterocyclic thiazole-bearing molecules. Additionally, they figured out that the highest inhibition effect was observed in the chloro-substituted compound with a rate of 46% [62]. Our compounds also comprise chloro-substituted species and showed similar activity.

3.9 | Cytotoxic Activity Studies

The data in Table 3 show cytotoxic activity results of compounds (**2b**, **2c**, **3a-c**) on various cancer cell lines (colon - DLD-1, lung - A549, liver - HepG2) with IC_{50} (half maximal

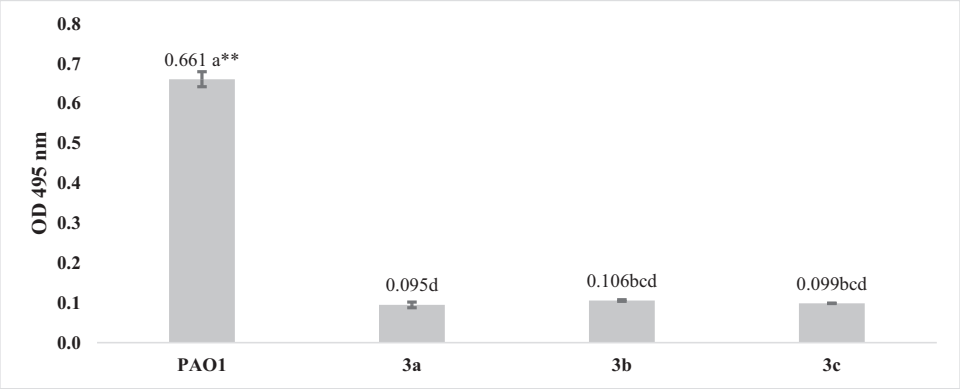

FIGURE 5 | Inhibition effect of molecules on P. *aeruginosa* PAO1 elastase production. **The difference between the means shown with different letters is statistically significant ($p < 0.01$).

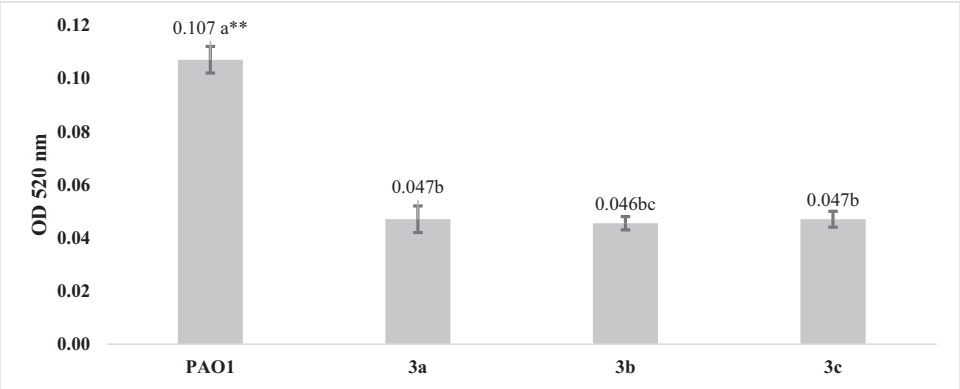

FIGURE 6 | Effect of synthesized molecules on *P. aeruginosa* PAO1 on pyocyanin pigment production. **The difference between the means shown with different letters is statistically significant ($p < 0.01$).

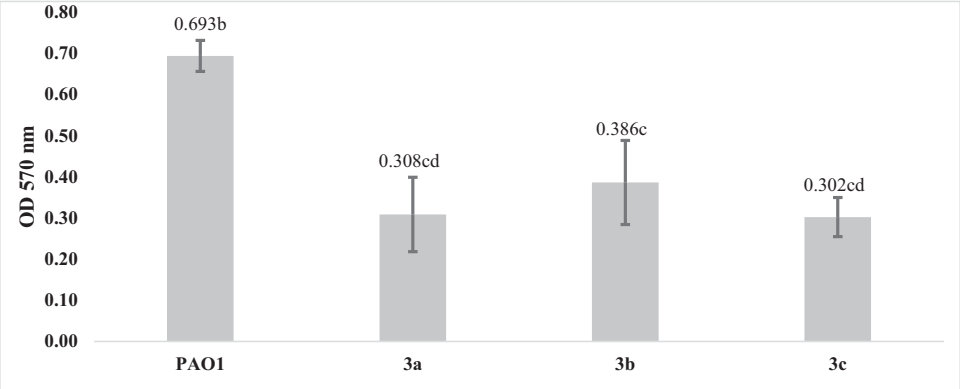

FIGURE 7 | Effect of molecules on biofilm formation in *P. aeruginosa*. **The difference between the means shown with different letters is statistically significant ($p < 0.01$).

inhibitory concentration) values. The IC_{50} value refers to the concentration required for a compound to inhibit cell growth. Lower IC_{50} values indicate that the compound is a more potent inhibitor.

The IC_{50} values of compound **2b** in lung (A549) and liver (HepG2) cancer cell lines were 123 μM and 150.5 μM, respectively. These results indicate that this compound has lower cytotoxic activity compared to other compounds. Compound **3b** prepared based on this compound (**2b**) was found to exhibit a higher cytotoxic effect in the same cell lines. Compound **3b** had IC_{50} values of 25.74 μM in DLD-1, 45.36 μM in A549, and 37.14 μM in HepG2 cell lines. These values indicate that compound **3b** is a potent inhibitor in all tested cell lines. The IC_{50} values of compound **2c** in A549 and HepG2 cell lines were 88.2 μM and 89.37 μM, respectively. These results show that it exhibits a slightly better activity compared to **2b**, but still displays lower inhibition compared to the other main products (**3a-c**). Compound **3c**, which was prepared based on compound **2c**, has IC_{50} values of 22.80 μM in the DLD-1 cell line, 38.18 μM

TABLE 3 | IC_{50} results for compounds in cancer cell lines.

Compounds	IC_{50} (μM)		
	DLD-1	A549	HepG2
2b	N.T.*	123.00	150.50
2c	N.T.*	88.20	89.37
3a	29.94	73.32	65.35
3b	25.74	45.36	37.14
3c	22.80	38.18	24.33
Cisplatin	9.79	16.24	73.69

N.T.*: Not tested.

in A549, and 24.33 μM in HepG2. This compound (**3c**) was detected to be the compound exhibiting the highest inhibition potential among the synthesized compounds. Among the main products, compound **3a** containing the benzyl groups showed the lowest cytotoxic effect. In the DLD-1 cell line, this compound demonstrated moderate activity with an IC_{50} value of 29.94 μM. In A549 and HepG2 cell lines, the IC_{50} values were 73.32 μM and 65.35 μM, respectively, indicating that this compound had a significant activity but inhibited the growth of cancer cells less than compound **3b** containing 2-methylbenzyl group and **3c** containing 2-chlorobenzyl group.

4 | Conclusion

A series of novel *N*,*N*-disubstituted-2-mercapto-benzimidazolium salts (compounds **3a-c**), in conjunction with two new benzimidazolium chlorides **2b** and **2c** have been prepared and identified through NMR and LC-MS spectroscopy. Subsequently, the cytotoxic capability and inhibitory effect of the aforementioned compounds were assessed. The relatively active compounds showed the potential to bind to the topo2α target. Their binding potential was less than the standard drug. The stability of the resulting complexes and the possibility of the compounds to remain inside the binding site were also measured. The enzyme-compound complexes obtained from the docking were stable generally. However, the status of the compounds to remain inside the binding site was different. In this respect, compounds **3a** and **3b** are anticipated to remain inside the binding site throughout the simulation time. Furthermore, the relatively active compounds are anticipated to have drug-like properties. On the other hand, all the inspected benzimidazolium salts (**3a-c**) demonstrated practically desirable inhibition effects, and the uppermost inhibitory proficiency was recognized on elastase production with an inhibition rate of 84-86%. The synthesized compounds were tested against three different cancer cell lines (A549, DLD-1, HepG2) and all compounds were found to have cytotoxic effect. However, among the synthesized compounds, compounds **3b** and **3c** had the highest activity in all three cell lines.

Author Contributions

Mohammad Mavvaji: formal analysis, investigation, resources, validation, visualization. **Muhammed Tilahun Muhammed:** formal analysis, methodology, visualization, resources, software, validation. **Ebru Onem:** investigation, formal analysis, resources, validation, visualization. **Halime Güzin Aslan:** funding acquisition, validation, project administration. **Sadeq K Alhag:** funding acquisition, validation, methodology. **Senem Akkoc:** funding acquisition, writing – original draft, writing – review and editing, formal analysis, project administration, resources, supervision, validation, visualization.

Acknowledgments

The authors would like to thank the Erciyes University Research Fund for financial support with project number FBA-2022-11424. MM and SA would also like to thank the Süleyman Demirel University postdoctoral research program (DOSAP-2022-8664) and Research Fund (TSG-2024-9516). S.K.A. appreciates the Deanship of Scientific Research at King Khalid University for funding this study through the Large Groups Project under grant number (R.G.P.2/31/46).

Conflicts of Interest

The authors declare no conflict of interest.

Data Availability Statement

The data that support the findings of this study are available from the corresponding author upon reasonable request. Data available on request from the authors.

References

1. A. Mehra and R. Sangwan, "Synthesis and Pharmacological Properties of the Benzimidazole Scaffold: A Patent Review," *ChemistrySelect* 8, no. 45 (2023): e202300537, https://doi.org/10.1002/slct.202300537.

2. Y. T. Lee, Y. J. Tan, and C. E. Oon, "Benzimidazole and Its Derivatives as Cancer Therapeutics: The Potential Role From Traditional to Precision Medicine," *Acta Pharmaceutica Sinica B* 13 (2023): 478–497, https://doi.org/10.1016/j.apsb.2022.09.010.

3. N. D. Mahurkar, N. D. Gawhale, M. N. Lokhande, S. J. Uke, and M. M. Kodape, "Benzimidazole: A Versatile Scaffold for Drug Discovery and Beyond-A Comprehensive Review of Synthetic Approaches and Recent Advancements In Medicinal Chemistry," *Results in Chemistry* 6 (2023): 101139, https://doi.org/10.1016/j.rechem.2023.101139.

4. N. J. Basha, "Therapeutic Efficacy of Benzimidazole and Its Analogs: An Update," *Polycyclic Aromatic Compounds* 43, no. 7 (2023): 6549–6569, https://doi.org/10.1080/10406638.2022.2118334.

5. C. S. W. Law and K. Y. Yeong, "Benzimidazoles In Drug Discovery: A Patent Review," *ChemMedChem* 16, no. 12 (2021): 1861–1877, https://doi.org/10.1002/cmdc.202100004.

6. L. A. Mohammed, M. A. Farhan, S. A. Dadoosh, et al., "A Review on Benzimidazole Heterocyclic Compounds: Synthesis and Their Medicinal Activity Applications," *SynOpen* 07, no. 04 (2023): 652–673, https://doi.org/10.1055/a-2155-9125.

7. K. Shabana, I. Salahuddin, A. Mazumder, et al., "Review on the Discovery of New Benzimidazole Derivatives as Anticancer Agents: Synthesis and Structure-Activity Relationship (2010-2022)," *Letters in Drug Design & Discovery* 21, no. 3 (2024): 451–479, https://doi.org/10.2174/1570180820666221017155955.

8. D. Meco, G. Attinà, S. Mastrangelo, P. Navarra, and A. Ruggiero, "Emerging Perspectives on the Antiparasitic Mebendazole as a Repurposed Drug for the Treatment of Brain Cancers," *International Journal of Molecular Sciences* 24, no. 2 (2023): 1334, https://doi.org/10.3390/ijms24021334.

9. M. Rahman, A. S. M. Saikat, M. Islam, M. Parvez, A. Khasru, and B. Kim, "Recent Update and Drug Target In Molecular and Pharmacological Insights Into Autophagy Modulation In Cancer Treatment and Future Progress," *Cells* 12, no. 3 (2023): 458, https://doi.org/10.3390/cells12030458.

10. M. Nardi, N. C. H. Cano, S. Simeonov, et al., "A Review on the Green Synthesis of Benzimidazole Derivatives and Their Pharmacological Activities," *Catalysts* 13, no. 2 (2023): 392, https://doi.org/10.3390/catal13020392.

11. K. Goyal, A. Sharma, R. Arya, R. Sharma, G. K. Gupta, and A. K. Sharma, "Double Edge Sword Behavior of Carbendazim: A Potent Fungicide With Anticancer Therapeutic Properties," *Anti-Cancer Agents in Medicinal Chemistry* 18 (2018): 38–45, https://doi.org/10.2174/1871520616666161221113623.

12. U. H. Jin, K. Karki, S. B. Kim, and S. Safe, "Inhibition of Pancreatic Cancer panc1 Cell Migration by Omeprazole Is Dependent on Aryl Hydrocarbon Receptor Activation of Jnk," *Biochemical and Biophysical Research Communications* 501 (2018): 751–757, https://doi.org/10.1016/j.bbrc.2018.05.061.

13. Z. Liu, J. Xiong, S. Gao, et al., "Ameliorating Cancer Cachexia by Inhibiting Cancer Cell Release of Hsp70 and Hsp90 With Omeprazole," *Journal of Cachexia, Sarcopenia and Muscle* 13 (2022): 636–647, https://doi.org/10.1002/jcsm.12851.

14. Z. Liu, J. Xiong, S. Gao, et al., "Ameliorating Cancer Cachexia by Inhibiting Cancer Cell Release of Hsp70 and Hsp90 With Omeprazole," *Journal of Cachexia, Sarcopenia and Muscle* 13 (2022): 636–647, https://doi.org/10.1002/jcsm.12851.

15. B. Gidwani and A. Vyas, "Formulation, Characterization and Evaluation of Cyclodextrin-Complexed Bendamustine-Encapsulated Plga Nanospheres for Sustained Delivery In Cancer Treatment," *Pharmaceutical Development and Technology* 21 (2016): 161–171, https://doi.org/10.3109/10837450.2014.979945.

16. J. S. S. M. Petersen and S. K. Baird, "Treatment of Breast and Colon Cancer Cell Lines With Anti-Helmintic Benzimidazoles Mebendazole or Albendazole Results In Selective Apoptotic Cell Death," *Journal of Cancer Research and Clinical Oncology* 147 (2021): 2945–2953, https://doi.org/10.1007/s00432-021-03698-0.

17. S. Venugopal, B. Kaur, A. Verma, et al., "Recent Advances of Benzimidazole as Anticancer Agents," *Chemical Biology & Drug Design* 102, no. 2 (2023): 357–376, https://doi.org/10.1111/cbdd.14236.

18. M. El-Naggar, W. M. Eldehna, H. Almahli, et al., "Novel Thiazolidinone/Thiazolo [3, 2-a] Benzimidazolone-Isatin Conjugates As Apoptotic Anti-Proliferative Agents Towards Breast Cancer: One-Pot Synthesis and In Vitro Biological Evaluation," *Molecules* 23 (2018): 1420, https://doi.org/10.3390/molecules23061420.

19. M. A. Shaldam, D. Hendrychová, R. El-Haggar, et al., "2, 4-Diarylpyrimido [1, 2-a] Benzimidazole Derivatives as Novel Anticancer Agents Endowed With Potent Anti-Leukemia Activity: Synthesis, Biological Evaluation and Kinase Profiling," *European Journal of Medicinal Chemistry* 258 (2023): 115610, https://doi.org/10.1016/j.ejmech.2023.115610.

20. A. A. M. Alkhaldi, M. M. Al-Sanea, A. Nocentini, et al., "3-Methylthiazolo [3, 2-a] Benzimidazole-Benzenesulfonamide Conjugates as Novel Carbonic Anhydrase Inhibitors Endowed With Anticancer Activity: Design, Synthesis, Biological and Molecular Modeling Studies," *European Journal of Medicinal Chemistry* 207 (2020): 112745, https://doi.org/10.1016/j.ejmech.2020.112745.

21. M. Mavvaji and S. Akkoc, "Recent Advances In the Anticancer Applications of Benzimidazole Derivatives," *ChemistrySelect* 8, no. 35 (2023): e202302561, https://doi.org/10.1002/slct.202302561.

22. M. Ali, S. Ali, M. Khan, et al., "Synthesis, Biological Activities, and Molecular Docking Studies of 2-mercaptobenzimidazole Based Derivatives," *Bioorganic Chemistry* 80 (2018): 472–479, https://doi.org/10.1016/j.bioorg.2018.06.032.

23. E. Vessally, R. Mohammadi, A. Hosseinian, K. Didehban, and L. Edjlali, "S-Arylation of 2-mercaptobenzazoles: A Comprehensive Review," *Journal of Sulfur Chemistry* 39, no. 4 (2018): 443–463, https://doi.org/10.1080/17415993.2018.1436712.

24. M. Faheem, A. Rathaur, A. Pandey, V. Kumar Singh, and A. K. Tiwari, "A Review on the Modern Synthetic Approach of Benzimidazole Candidate," *ChemistrySelect* 5, no. 13 (2020): 3981–3994, https://doi.org/10.1002/slct.201904832.

25. H. E. Hashem and Y. El Bakri, "An Overview on Novel Synthetic Approaches and Medicinal Applications of Benzimidazole Compounds," *Arabian Journal of Chemistry* 14, no. 11 (2021): 103418, https://doi.org/10.1016/j.arabjc.2021.103418.

26. V. A. S. Pardeshi, N. S. Chundawat, S. I. Pathan, P. Sukhwal, T. P. S. Chundawat, and G. P. Singh, "A Review on Synthetic Approaches of Benzimidazoles," *Synthetic Communications* 51, no. 4 (2021): 485–513, https://doi.org/10.1080/00397911.2020.1841239.

27. D. Chinemerem Nwobodo, M. C. Ugwu, C. Oliseloke Anie, et al., "Antibiotic Resistance: The Challenges and Some Emerging Strategies for Tackling a Global Menace," *Journal of Clinical Laboratory Analysis* 36, no. 9 (2022): e24655, https://doi.org/10.1002/jcla.24655.

28. T. Boban, S. Nadar, and S. Tauro, "Breaking down Bacterial Communication: a Review of Quorum Quenching Agents," *Future Journal of Pharmaceutical Sciences* 9 (2023): 77, https://doi.org/10.1186/s43094-023-00526-9.

29. B. F. Minaev, "Electronic Mechanisms of Activation of Molecular Oxygen," *Russian Chemical Reviews* 76, no. 11 (2007): 1059–1083, http://iopscience.iop.org/0036-021X/76/11/R01.

30. R. H. Abd El-Aleam, A. M. Sayed, M. N. Taha, R. F. George, H. H. Georgey, and H. M. Abdel-Rahman, "Design and Synthesis of Novel Benzimidazole Derivatives As Potential Pseudomonas Aeruginosa Anti-Biofilm Agents Inhibiting Lasr: Evidence from Comprehensive Molecular Dynamics Simulation and In Vitro Investigation," *European Journal of Medicinal Chemistry* 241 (2022): 114629, https://doi.org/10.1016/j.ejmech.2022.114629.

31. N. Durán and C. F. M. Menck, "Chromobacterium Violaceum: A Review of Pharmacological and Industiral Perspectives," *Critical Reviews in Microbiology* 27, no. 3 (2001): 201–222, https://doi.org/10.1080/20014091096747.

32. D. Alem, J. J. Marizcurrena, V. Saravia, D. Davyt, W. Martinez-Lopez, and S. Castro-Sowinski, "Production and Antiproliferative Effect of Violacein, a Purple Pigment Produced by an Antarctic Bacterial Isolate," *World Journal of Microbiology and Biotechnology* 36 (2020): 120 , https://doi.org/10.1007/s11274-020-02893-4.

33. K. Poole, "Pseudomonas Aeruginosa: Resistance to the Max," *Frontiers in Microbiology* 2 (2011): 65, https://doi.org/10.3389/fmicb.2011.00065.

34. M. Mavvaji, C. Tuğrul Zeyrek, and S. Akkoc, "Investigation of the Cytotoxic Activity, Dft Calculation, and Docking Studies Newly Synthesized 1,3-disubstituted Benzimidazolium Chlorides on Human Liver Cancer, Lung Cancer, and Normal Embryonic Kidney Cell Lines," *Biochemical and Biophysical Research Communications* 741 (2024): 151024, https://doi.org/10.1016/j.bbrc.2024.151024.

35. S. Akkoç, İ. Özer İlhan, Y. Gök, P. J. Upadhyay, and V. Kayser, "In Vitro Cytotoxic Activities of New Silver and Peppsi Palladium N-Heterocyclic Carbene Complexes Derived From Benzimidazolium Salts," *Inorganica Chimica Acta* 449 (2016): 75–81, https://doi.org/10.1016/j.ica.2016.05.001.

36. S. Akkoç, Y. Gök, İ. Ö. İlhan, and V. Kayser, "N-Methylphthalimide-Substituted Benzimidazolium Salts and Peppsi Pd–Nhc Complexes: Synthesis, Characterization and Catalytic Activity In Carbon-Carbon Bond-Forming Reactions," *Beilstein Journal of Organic Chemistry* 12, no. 1 (2016): 81–88, https://doi.org/10.3762/bjoc.12.9.

37. S. Akkoç, V. Kayser, İ. Ö. İlhan, et al., "New Compounds Based on a Benzimidazole Nucleus: Synthesis, Characterization and Cytotoxic Activity Against Breast and Colon Cancer Cell Lines," *Journal of Organometallic Chemistry* 839 (2017): 98–107, https://doi.org/10.1016/j.jorganchem.2017.03.037.

38. S. Akkoç, "Antiproliferative Activities of 2-hydroxyethyl Substituted Benzimidazolium Salts and Their Palladium Complexes against Human Cancerous Cell Lines," *Synthetic Communications* 49, no. 21 (2019): 2903–2914, https://doi.org/10.1080/00397911.2019.1650187.

39. S. Akkoç, V. Kayser, and İ. Ö. İlhan, "Synthesis Andin Vitroanticancer Evaluation of Some Benzimidazolium Salts," *Journal of Heterocyclic Chemistry* 56, no. 10 (2019): 2934–2944, https://doi.org/10.1002/jhet.3687.

40. S. Akkoç, "Derivatives of 1-(2-(Piperidin-1-yl) ethyl)-1H-benzo [D] Imidazole: Synthesis, Characterization, Determining of Electronic Properties and Cytotoxicity Studies," *ChemistrySelect* 4, no. 17 (2019): 4938–4943, https://doi.org/10.1002/slct.201900353.

41. S. Akkoç, "Design, Synthesis, Characterization, and In Vitro Cytotoxic Activity Evaluation of 1, 2-disubstituted Benzimidazole Compounds," *Journal of Physical Organic Chemistry* 34, no. 1 (2021): e4125, https://doi.org/10.1002/poc.4125.

42. M. Mavvaji, M. T. Muhammed, and S. Akkoc, "Synthesis, Cytotoxic Activity, Docking and Md Simulation of *N*, *N*-Disubstituted New Benzimidazolium Salts," *ChemistrySelect* 8, no. 43 (2023): e202303053, https://doi.org/10.1002/slct.202303053.

43. N. Jeremias, L. M. Mohr, and T. Bach, "Intermolecular [2+2] Photocycloaddition of α, β-unsaturated Sulfones: Catalyst-Free Reaction and Catalytic Variants," *Organic Letters* 23, no. 15 (2021): 5674–5678, https://doi.org/10.1021/acs.orglett.1c01794.

44. Y. R. Wang, S. F. Chen, C. C. Wu, et al., "Producing Irreversible Topoisomerase Ii-Mediated Dna Breaks By Site-Specific Pt(Ii)-Methionine Coordination Chemistry," *Nucleic Acids Research* 45, no. 18 (2017): 10861–10871, https://doi.org/10.1093/nar/gkx742.

45. S. Kim, J. Chen, T. Cheng, et al., "Pubchem In 2021: New Data Content and Improved Web Interfaces," *Nucleic Acids Research* 49, no. D1 (2021): D1388–D1395, https://doi.org/10.1093/nar/gkaa971.

46. O. Trott and A. J. Olson, "Autodock Vina: Improving the Speed and Accuracy of Docking with a New Scoring Function, Efficient Optimization and Multithreading," *Journal of Computational Chemistry* 31, no. 2 (2010): 455–461, https://doi.org/10.1002/jcc.21334.

47. M. T. Muhammed and E. Aki-Yalcin, "Computational Insight into the Mechanism of Action of Dna Gyrase Inhibitors; Revealing a New Mechanism," *Current Computer-Aided Drug Design* 20, no. 3 (2024): 224–235, https://doi.org/10.2174/1573409919666230419094700.

48. M. T. Muhammed, Z. Kokbudak, and S. Akkoc, "Cytotoxic Activities of the Pyrimidine-Based Acetamide and Isophthalimide Derivatives: An In Vitro and In Silico Studies," *Molecular Simulation* 49, no. 10 (2023): 982–992, https://doi.org/10.1080/08927022.2023.2202766.

49. B. Gökçe and M. T. Muhammed, "Evaluation of In Vitro Effect, Molecular Docking, and Molecular Dynamics Simulations of Some Dihydropyridine-Class Calcium Channel Blockers on Human Serum Paraoxonase 1 (hPON1) Enzyme Activity," *Biotechnology and Applied Biochemistry* 70, no. 5 (2023): 1707–1719, https://doi.org/10.1002/bab.2467.

50. A. Daina, O. Michielin, and V. Zoete, "Swissadme: A Free Web Tool to Evaluate Pharmacokinetics, Drug-Likeness and Medicinal Chemistry Friendliness of Small Molecules," *Scientific Reports* 7, no. 1 (2017): 42717, https://doi.org/10.1038/srep42717.

51. J. M. Andrews, "Determination of Minimum Inhibitory Concentrations," *Journal of Antimicrobial Chemotherapy* 48 (2001): 5–16, https://doi.org/10.1093/jac/48.suppl_1.5.

52. D. Anbazhagan, M. Mansor, G. O. S. Yan, M. Y. Md Yusof, H. Hassan, and S. D. Sekaran, "Detection of Quorum Sensing Signal Molecules and Identification of an Autoinducer Synthase Gene Among Biofilm Forming Clinical Isolates of Acinetobacter Spp," *PLoS One* 7, no. 7 (2012): e36696, https://doi.org/10.1371/journal.pone.0036696.

53. D. E. Ohman, S. J. Cryz, and B. H. Iglewski, "Isolation and Characterization of Pseudomonas Aeruginosa Pao Mutant That Produces Altered Elastase," *Journal of Bacteriology* 142 (1980): 836–842, https://doi.org/10.1128/jb.142.3.836-842.1980.

54. D. W. Essar, L. Eberly, A. Hadero, and I. P. Crawford, "Identification and Characterization of Genes for a Second Anthranilate Synthase In Pseudomonas Aeruginosa: Interchangeability of the Two Anthranilate Synthases and Evolutionary Implications," *Journal of Bacteriology* 172 (1990): 884–900, https://doi.org/10.1128/jb.172.2.884-900.1990.

55. G. A. O'Toole, "Microtiter Dish Biofilm Formation Assay," *Journal of Visualized Experiments : JoVE* 30, no. 47 (2011): 2437, https://doi.org/10.3791/2437.

56. T. Ertan-Bolelli and K. Bolelli, "Discovery of New Dna Topoisomerase Ii Inhibitors Using Structure Based Virtual Screening Method," *J. Turk. Chem. Soc.: Sect. A* 6 (2019): 71–78, https://doi.org/10.18596/jotcsa.466457.

57. R. M. Linka, A. C. G. Porter, A. Volkov, C. Mielke, F. Boege, and M. O. Christensen, "C-Terminal Regions of Topoisomerase Ii α and Ii β Determine Isoform-Specific Functioning of the Enzymes In Vivo," *Nucleic Acids Research* 35 (2007): 3810–3822, https://doi.org/10.1093/nar/gkm102.

58. C. C. Wu, T. K. Li, L. Farh, et al., "Structural Basis of Type Ii Topoisomerase Inhibition By the Anticancer Drug Etoposide," *Science* 333, no. 6041 (2011): 459–462, https://doi.org/10.1126/science.1204117.

59. S. Y. van der Zanden, X. Qiao, and J. Neefjes, "New Insights into the Activities and Toxicities of the Old Anticancer Drug Doxorubicin," *The FEBS journal* 288, no. 21 (2021): 6095–6111, https://doi.org/10.1111/febs.15583.

60. I. Celik, M. Erol, and Z. Duzgun, "In Silico Evaluation of Potential Inhibitory Activity of Remdesivir, Favipiravir, Ribavirin and Galidesivir Active Forms on SARS-CoV-2 Rna Polymerase," *Molecular Diversity* 26, no. 1 (2022): 279–292, https://doi.org/10.1007/s11030-021-10215-5.

61. M. T. Muhammed, M. Er, and S. Akkoc, "Molecular Modeling and In Vitro Antiproliferative Activity Studies of Some Imidazole and Isoxazole Derivatives," *Journal of Molecular Structure* 1282 (2023): 135066, https://doi.org/10.1016/j.molstruc.2023.135066.

62. C. A. Lipinski, F. Lombardo, B. W. Dominy, and P. J. Feeney, "Experimental and Computational Approaches to Estimate Solubility and Permeability In Drug Discovery and Development Settings," *Advanced Drug Delivery Reviews* 46, no. 1–3 (2001): 3–26, https://doi.org/10.1016/S0169-409X(00)00129-0.

63. S. Mao, Q. Li, Z. Yang, Y. Li, X. Ye, and H. Wang, "Design, Synthesis, and Biological Evaluation of Benzoheterocyclic Sulfoxide Derivatives As Quorum Sensing Inhibitors In *Pseudomonas Aeruginosa*," *Journal of Enzyme Inhibition and Medicinal Chemistry* 38, no. 1 (2023): 2175820, PMID: 36748317; PMCID: PMC9930800, https://doi.org/10.1080/14756366.2023.2175820.

64. T. Morohoshi, T. Shiono, K. Takidouchi, et al., "Inhibition of Quorum Sensing In Serratia Marcescens As-1 By Synthetic Analogs of *N*-Acylhomoserine Lactone," *Applied and Environmental Microbiology* 73, no. 20 (2007): 6339–6344, https://doi.org/10.1128/AEM.00593-07.

65. J. Lee and L. Zhang, "The Hierarchy Quorum Sensing Network In *Pseudomonas Aeruginosa*," *Protein & Cell* 6, no. 1 (2015): 26–41, https://doi.org/10.1007/s13238-014-0100-x.

66. G. Xiao, J. He, and L. G. Rahme, "Mutation Analysis of the Pseudomonas Aeruginosa Mvfr and Pqsabcde Gene Promoters Demonstrates Complex Quorum-Sensing Circuitry," *Microbiology* 152, no. 6 (2006): 1679–1686, https://doi.org/10.1099/mic.0.28605-0.